Numerical Evaluation of Flow and Performance of Turbo Pump Inducers

Chang-Yeul Shim
Seoul National University, Turbo and Power Machinery Research Center, Shillim-dong, Kwanak-gu, Seoul 151-742, Korea
Shin-Hyoung Kang*
School of Mechanical and Aerospace Engineering Seoul National University, Shillim-dong, Kwanak-gu, Seoul 151-742, Korea

Steady state flow calculations are executed for turbo-pump inducers of modern design to validate the performance of Tascflow code. Hydrodynamic performance of inducers is evaluated and structure of the passage flow and leading edge recirculation are also investigated. Calculated results show good coincidence with experimental data of static pressure performance and velocity profiles over the leading edge. Upstream recirculation, tip leakage and vortex flow at the blade tip and near leading edge are main sources of pressure loss. Amount of pressure loss from the upstream to the leading edge corresponds to that of whole pressure loss through the blade passage. The viscous loss is considerably large due to the strong secondary flow. There appears more stronger leading edge recirculation for the backswept inducer, and this increases the pressure loss. However, blade loading near the leading edge is considerably reduced and cavitation inception delayed.

Key Words : Turbo Pump, Inducer, Pressure Loss, Secondary Flow, Recirculation

Nomenclature

c : Absolute velocity
p : Static pressure
p_t : Total pressure
p_0 : Total pressure at inlet
r : Radius
r_h : Hub radius
r_t : Shroud radius
R : Spanwise fraction $(=r-r_h/r_t-r_h)$
u_t : Rotational speed of inducer tip
w : Relative velocity
β : Blade angle
ρ : Density
ω : Angular velocity of inducer
ϕ : Flow coefficient $(=c_{mt}/u_t)$
ψ : Pressure coefficient $(=gH/(\rho u_t^2))$
σ : Cavitation number $(=(p_t-p_v)/0.5u_t^2)$
t : Tangential component
z : Axial component
m : Meridional component
1 : Value at inducer inlet
2 : Value at inducer exit

* Corresponding Author,
E-mail : kangsh@snu.ac.kr
TEL : +82-2-880-7118; **FAX** : +82-2-883-0179
School of Mechanical and Aerospace Engineering Seoul National University, Shillim-dong, Kwanak-gu, Seoul 151-742, Korea. (Manuscript **Received** July 24, 2002; **Revised** January 12, 2004)

1. Introduction

An inducer is an important element in many high speed pumps for commercial and aerospace applications. The turbo pump inducer for rocket propulsion engine affects hydrodynamic performance and cavitation. Furthermore non-uniform incoming flow and cavitation induced vibration of the inducer blades, which is a critical aspect for safe operation of pumps.

Since the through flow is very complex, inducers are usually designed based on empirical

or semi-empirical techniques. Well developed CFD techniques are successfully used for modern turbomachinery design. However, numerical prediction of inception and growth of cavitation is still hard job. Even without the cavitation, the flow through the inducer is highly three dimensional one with strong viscous effects. Three dimensional viscous flow calculation is emerging as a tool facilitating improved designs (George, 1994). However, there are still needs of code validation due to difficulty of grid generation for blades of small angle and its sensitivity to the simulated results.

The structure of passage flow with strong secondary motion and leading edge recirculation has not been understood in detail until now. Dynamic modeling of the leading edge recirculation and its effect on the inducer performance are important research topics.

In this paper, numerical calculations are executed for turbo-pump inducers of modern design. The performance and flows measured by Tsujimoto and Yoshida (1998) are compared with the calculations using TascFlow. The structure of the passage flow and leading edge recirculation are also investigated.

2. Inducer Model

Shape of the inducer of radial blades is shown in Fig. 1. The model was designed based on the liquid oxygen turbopump of the LE-7 main engine of H-II rocket. This inducer has four helical blades with sharp leading edge and trailing edge, and blade wrap angel is 290 deg. The inlet blade angle, β_{t1} is 7.5 deg. and outlet blade angle, β_{t2} is 9.0 deg. at the tip. The blade thickness at the tip is 2 mm and the leading edge radius 0.2 mm. The solidity is 2.97 at the tip, and variation of the blade angle, with the radius, r is designed following $r \tan \beta$=constant. Table 1 shows a specification of the inducer in detail. A backswept model is also adopted in the study. The model is designed by cutting the radial leading edge (Tsujimoto et al., 2001).

2.1 Computational grid

The computational domain consists of 93,960 nodes (120 streamwise, 27 radial and 29 circumferential nodes), and Fig. 2 shows a meridional view of the calculation grid. The grids are generated using Turbo-Grid code (AEA Technology, 1999). One blade to blade space is modeled assuming the flow is periodic. Multi-block system is adopted to avoid high skewness of the cells. Fine grids are allocated near the solid walls for the wall function boundary condition to be used.

Table 1 Specifications of the inducer

Tip diameter	149.8 mm
Inlet tip blade angle	7.5 deg
Outlet tip blade angle	9.0 deg
Hub/tip ratio at inlet	0.25
Hub/tip ratio at outlet	0.51
Tip clearance	0.5 mm
Blade thickness at tip	2 mm
Blade thickness at inlet hub	6 mm
Leading edge radius	0.2 mm
Solidity at tip	2.97

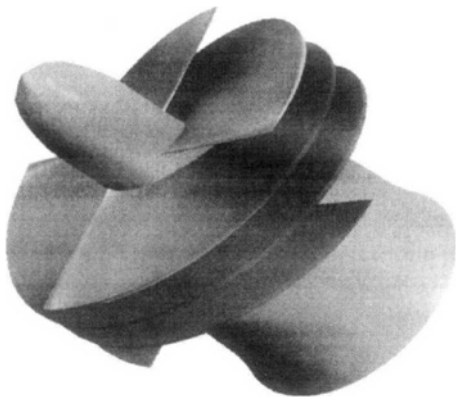

Fig. 1 Three dimensional view of the inducer

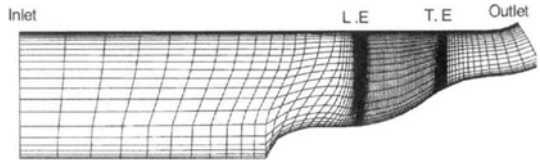

Fig. 2 Meridional view of computational grids

The calculation is performed with the relative frame of reference fixed to the rotation blade and the stationary frame of reference at the upstream and downstream of the inducer. The calculation domain is extended about 200 mm upstream from the leading edge to investigate recirculation that may appear at some flow-rates less than the design flow rate.

Five grid layers are allocated to obtain meaningful results of the tip clearance flow.

2.2 Boundary conditions

A simplified figure of the test section of the inducer is shown in Fig. 3. Axial coordinate is measured from the leading edge of the blades. The inducer blade and the hub wall are rotating with zero relative velocity. The casing, from the inlet to the exit, is a stationary wall with zero absolute velocity. The inlet flow is modeled as uniform axial flow with stagnation pressure specified. At the exit boundary, the flow rate is specified. The rotational speed is 4,000 rpm and working fluid is water.

The standard κ-ε turbulence model is used. The wall function option is used for the tangential velocity near the solid walls. The inlet turbulence intensity is assumed to be 5% and turbulent eddy viscosity is ten times of fluid viscosity.

3. Calculation Results

3.1 Calculated and measured performance

Calculations were performed for five different flow rates, the design flow coefficient of 0.078 and the off-design flow coefficients of 0.04, 0.05, 0.06, 0.07. Reynolds number based on the tip diameter and inlet axial velocity is 370,000. The calculation is finished when the residual of momentum becomes less than 1.3×10^{-4}.

The pressure rise performance is the most fundamental quantity to validate the code performance. Fig. 4 shows performance curve of static pressure coefficient for non-cavitating conditions measured by Tsujimoto and Yoshida (1998). The exit pressure was measured at $z=72$ mm as shown in Fig. 3. For the radial inducer, the difference between calculated and measured performance is less than 5%. The accuracy of calculation is very high.

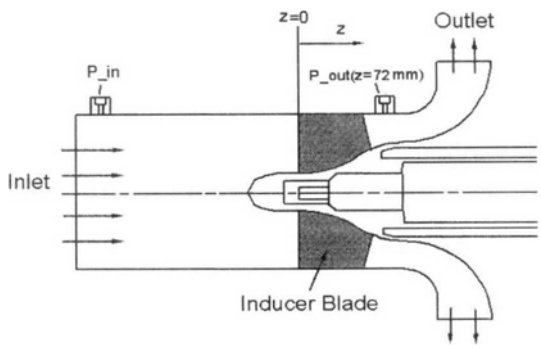

Fig. 3 Inducer cross section and the locations of flow measurements

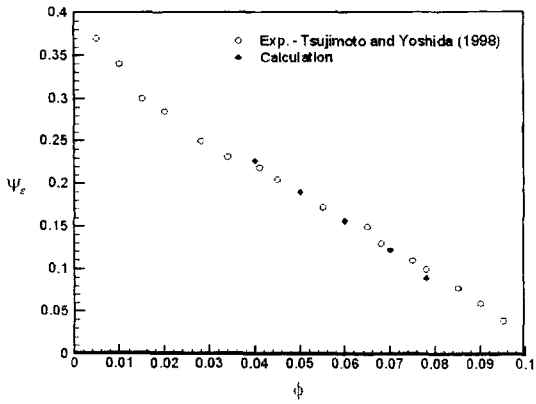

Fig. 4 Measured and calculated variations ofstatic pressure coefficients of radial inducer

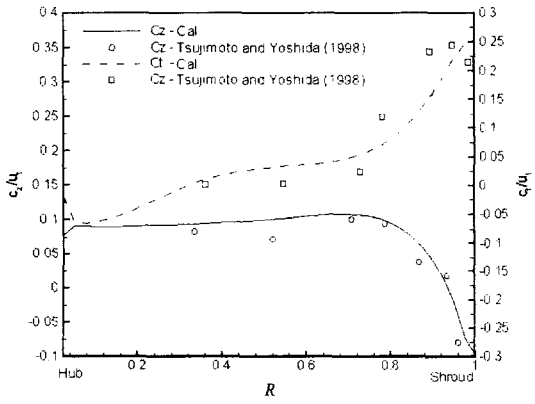

Fig. 5 Distributions of axial and tangential velocities at $z=-15$ mm ; $\phi=0.07$

There usually appears a recirculation flow over the leading edge even at the design flow rate and the size grows as the flow reduces. Figure 5 shows radial variations of axial and tangential velocity profiles at $z=-15$ mm (note that $z=0$ mm at leading edge) for the flow coefficient $\phi=0.07$. The flow was measured by Tsujimoto and Yoshida (1998), using a LDV system. The velocity profiles are circumferentially averaged values and non-dimensionalized by the inducer tip speed. Axial and tangential velocity profiles show good coincidence in the entire radial span from the hub to shroud.

The calculated and measured contours of axial velocity at $z=-5$ mm for the flow coefficient 0.07 are shown in Fig. 6. The comparison between calculated and measured distributions shows good coincidence. Consequently Fig. 5 and Fig. 6 show that the leading edge recirculation is successfully simulated in the present calculation.

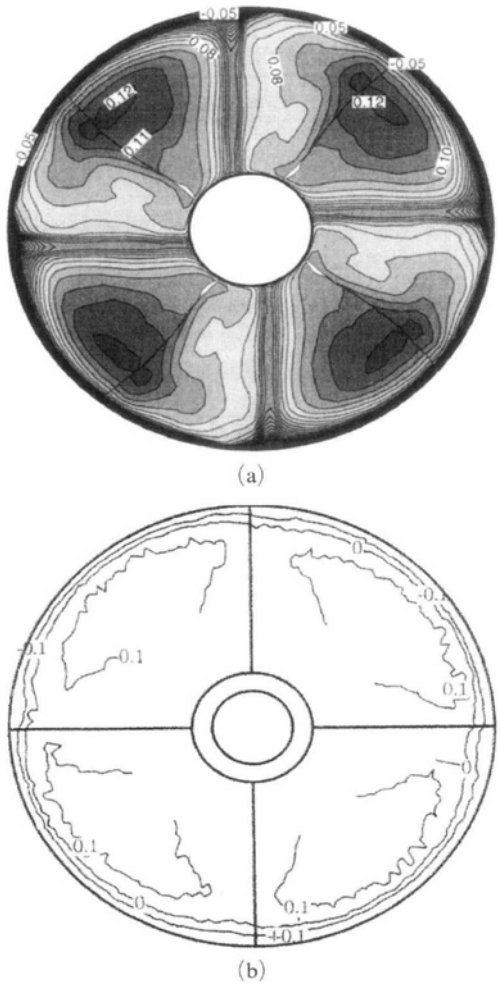

Fig. 6 (a) Calculated and (b) Measured contours of axial velocity at $z=-5$ mm ; $\phi=0.07$

3.2 Pressure and loss coefficients

Integrated parameters used in the design and one-dimensional analysis can be evaluated using results of through flow calculation. Total pressure p_t and rotary stagnation pressure, p^* are defined as follows respectively (Moore et al., 1995a)

$$p_t=p+\rho\cdot c^2/2 \tag{1}$$

$$p^*=p+\rho\cdot w^2/2-\omega^2 r^2/2 \tag{2}$$

Static and total pressure coefficients and loss coefficient are defined as follows ;

$$\psi_s=\frac{p-p_o}{\rho\cdot u_t^2} \tag{3}$$

$$\psi_t=\frac{p_t-p_o}{\rho\cdot u_t^2} \tag{4}$$

$$\psi_{loss}=\frac{p_o-p^*}{\rho\cdot u_t^2} \tag{5}$$

Defects in rotary stagnation pressure coefficient ψ_{loss}, represents the viscous loss through the rotor (Moore et al., 1995a, 1995b).

Rate of change in moment of momentum corresponds to work done without pressure loss, and moment of momentum coefficient is defined dimensionless as the following equation.

$$\psi_E=u_2c_{t2}/u_t^2 \tag{6}$$

where c_t is tangential velocity component. The total pressure coefficient can be obtained subtracting the loss from the Eq. (6).

$$\psi_t=\psi_E-\psi_{loss} \tag{7}$$

3.3 Meridional variations of pressure and loss

Variations of pressure coefficients, pressure loss and moment of momentum coefficients defined in Eqs. (3) ~ (6) are shown in Fig. 7 for the design flow rate and in Fig. 8 for the off-design

flow rates. At the design flow rate, moment of momentum coefficient gradually increases from the upstream to the exit of the inducer. Note that the value is non-zero at the leading edge, which is due to the rotating recirculation flow induced by the inducer. Pressure loss coefficient increases to 0.035 from the upstream to the leading edge of the blade and then increases to 0.07 through the blade passage. The amount of pressure loss before the leading edge is corresponding to that through the blade passage. Pressure loss before the leading edge is an important source of the total inducer loss. Pressure loss in the blade passage has a relatively high value showing that viscous effect is important in the blade passage flow. Variation of static pressure coefficients is obtained subtracting the dynamic head from the total pressure from Eq. (7). Contributions of each component to the final value of static pressure can be observed from the values at the inducer exit.

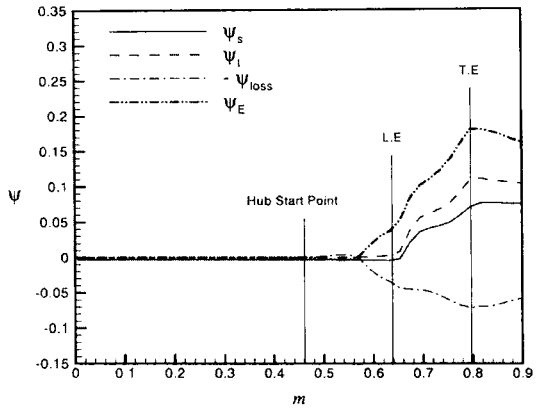

Fig. 7 Meridional variations of pressure and loss coefficients ; $\phi=0.078$

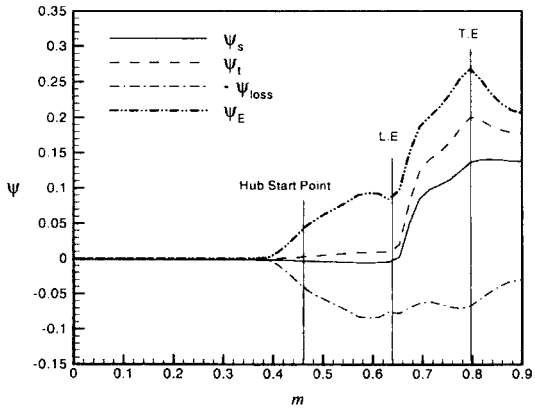

Fig. 8 Meridional variations of pressure and loss coefficients ; $\phi=0.06$

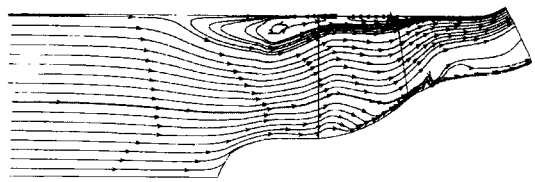

Fig. 9 Stream lines at the mid-passage ; $\phi=0.06$

On the other hand, as the flow rate decreases, the pressure loss at the upstream is very high and loss through the passage relatively becomes small as shown in Fig. 8. This is due to the strong upstream recirculation flow shown in Fig. 9, which also contributes to the moment of momentum coefficient. Pressure loss in front of leading edge due to backflow is extending toward upstream and growing up into the blade passage as shown in Fig. 9.

3.4 Pressure loss over the blade tip

The distribution of pressure loss can be observed in the meridional views of contours of rotary stagnation pressure in Fig. 10(a) for the design and (b) for the off-design flow rates. The

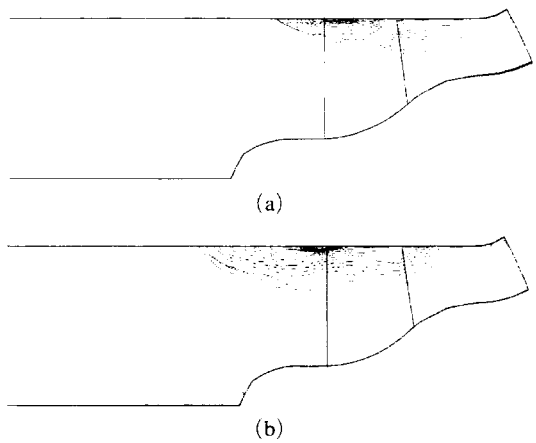

Fig. 10 Pressure loss coefficient contour at meridional surface for (a) Design flow rate, $\phi=$ 0. 078 and (b) Off-design flow rate, $\phi=0.06$

figures are pressure loss coefficient contour of $\psi_{loss}>0.06$ on the mid-passage plane. The pressure loss intensively distributes over the leading edge recirculation region as shown in Fig. 9 and blade tip region. Pressure loss near the blade tip is due to leakage flow through the blade tip clearance as shown in Fig. 11.

Figure 11 shows streamlines passing the blade tip. At the tip, there are three dominant types of flow ; recirculating flow, leakage flow and vortex flow. Tip-clearance flow near the leading edge flows pitchwise and bounces at the adjacent blade so that it constructs back flow at the blade leading edge. However, over one third downstream of the blade passage, the leakage flow goes to the downstream and pass over the next blade again. The streamlines at the further downstream move radially inward the passage so that it constructs vortex flow shown in Fig. 11.

3.5 Secondary flow in the blade passage

Figure 12 shows streamlines on the three meridional planes, (a) over the mid passage, (b) near the pressure surface, (c) near the suction surface for the design flow rate. Backflow is observed before the blade tip on all the planes. At the mid-passage Fig. 12(a) shows the development of radially inward flows, while near the pressure and suction surfaces radially outward flows appear, in the blade passage, as shown in Fig. 12(b) and (c). These figures show the secondary flow in the radial direction in the blade passage. Pressure distribution in the Fig. 13 shows its local minimum value near the leading edge and increases to the downstream.

The passage flow can be observed near an exit plane shown in Fig. 14(a). There is leakage flow from the pressure side to the suction side at the tip and it is mixed with the passage vortex as shown in Fig. 14(b). The leakage flow mixing with the passage flow near the suction side of tip generates high pressure loss at the tip region. There appears a big passage vortex near the suction-hub corner.

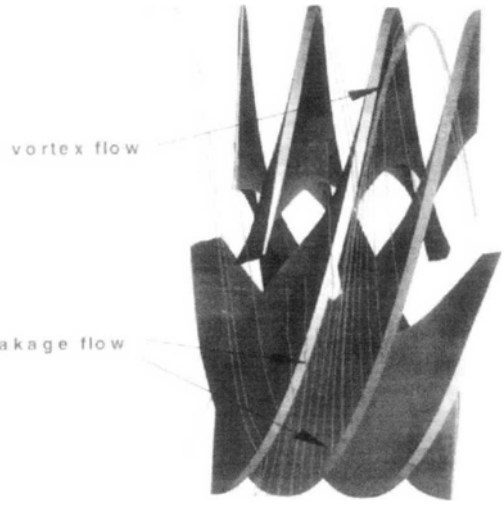

Fig. 11 Three dimensional view of streamlines passing the blade tip

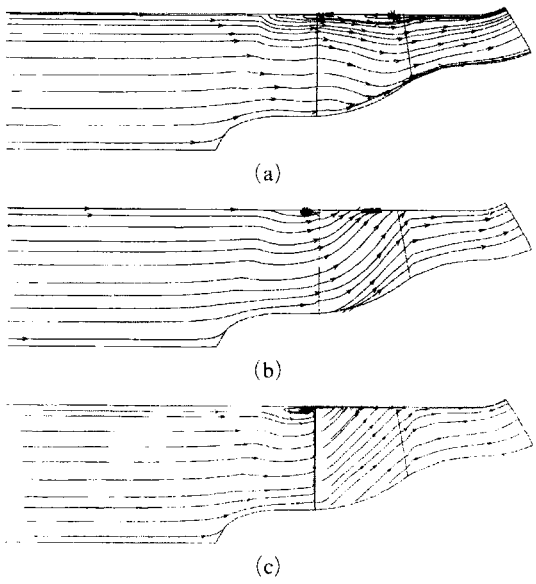

Fig. 12 Streamlines at (a) Near mid-passage, (b) Near pressure side, (c) Near suction side ; $\phi=0.078$

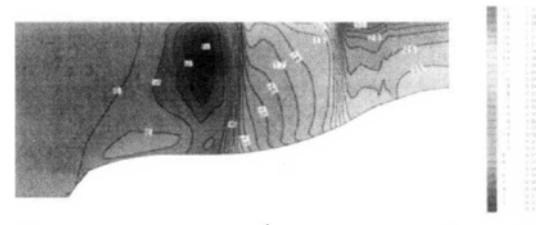

Fig. 13 Static pressure coefficient distribution at the meridional plane ; $\phi=0.078$

3.6 Variation of velocity and pressure profile at exit

Averaged velocity and flow angle distributions at the inducer exit are important for flow matching in the design of main impeller. At the exit plane, $z=62$ mm, the velocity and pressure coefficients are shown in Figs. 15 and 16. Fig. 15 shows the radial variations of meridional and tangential velocities at three flow rates, $\phi=0.078$, 0.07, 0.06. The meridional velocity is constant near the shroud for all flow rates, but near the hub it decreases as the flow rate decreases. It can be explained by increase of boundary layer due to relatively small velocity along the hub. As approaching to the shroud, the rotational speed increases and the blade angle decreases while meridional velocity has constant value, so that the tangential velocity increases. Figure 16 shows the variation of static and total pressure coefficients. Static pressure is slowly increasing but total pressure increases very rapidly to radial direction.

3.7 Backswept inducer

Backswept inducer is usually adopted for low tip loading and hydrodynamic performance. Tsujimoto and Yoshida (1998) also measured flows and performance for a model of backward sweep angle of 35.4 degree at the tip (Tsujimoto et al., 2001). The details of specification are not included here, but schematic contours are shown in Figs. 19 and 20. Two models do not show any meaningful difference in performance and local recirculation. Figure 17 shows the calculated

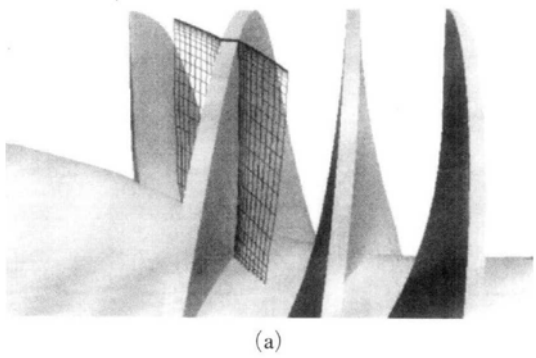

(a)

(b)

Fig. 14 (a) A plane near the blade exit and (b) Secondary flow and pressure loss ; $\phi=0.078$

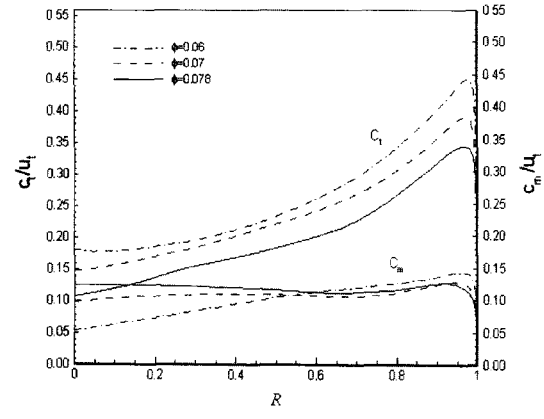

Fig. 15 Variations of velocity profile at the exit of the inducer ; $z=62$ mm

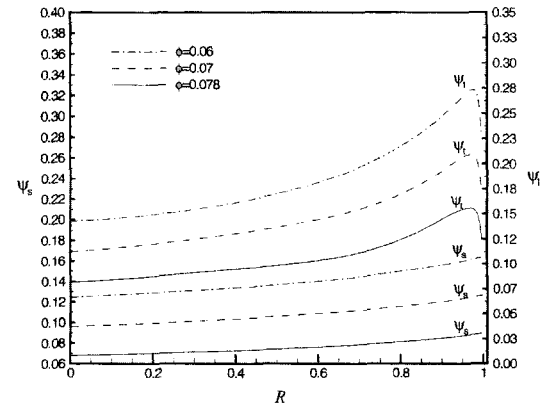

Fig. 16 Variations of pressure profile at the exit of the inducer ; $z=62$ mm

meridional variations of pressure and loss coefficients for the backswept model for the flow coefficient of 0.078. Comparing with the results of radial inducer shown in Fig. 7, the moment of momentum coefficient of the backswept inducer has similar value with that of the radial inducer, however larger values near the leading edge. Near the leading edge the pressure loss coefficient of the backswept inducer has higher than that of the radial inducer by 0.04, and also has higher value in the blade passage. It is due to relatively larger recirculation region in front of the leading edge shown in Fig. 18, and for this reason total pressure increases with relatively lower initial value at the leading edge than that of the radial inducer through the blade passage.

3.8 Blade loading

The static pressure coefficient distributions on the pressure and suction surfaces, together with their difference, i.e. the blade loading are shown in Fig. 19 for the radial vane and in Fig. 20 for the backswept vane, for the design flow coefficient, $\phi=0.078$. Such distributions are very difficult to experimentally obtain.

For the radial inducer vane, the pressure on the pressure surface gradually increases from values of 0.025 near the leading edge to about 0.046 at the exit type as shown in Fig. 19(a), while the pressure on the suction side gradually increases after showing its minimum value of -0.037 near the tip in Fig. 19(b), where the local maximum value of the blade loading locates in the Fig. 19(c).

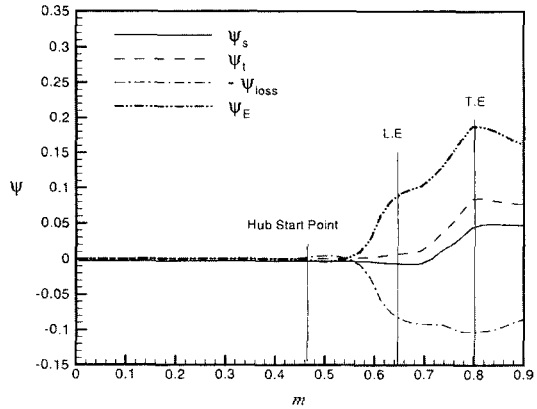

Fig. 17 Meridional variations of pressure and loss coefficients of the backswept model ; $\phi=$ 0.078

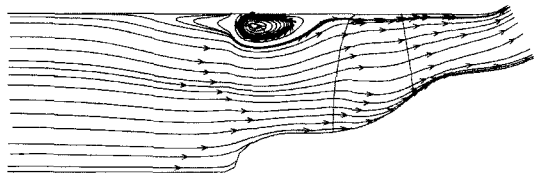

Fig. 18 Streamlines at the mid-passage of the backswept model ; $\phi=0.078$

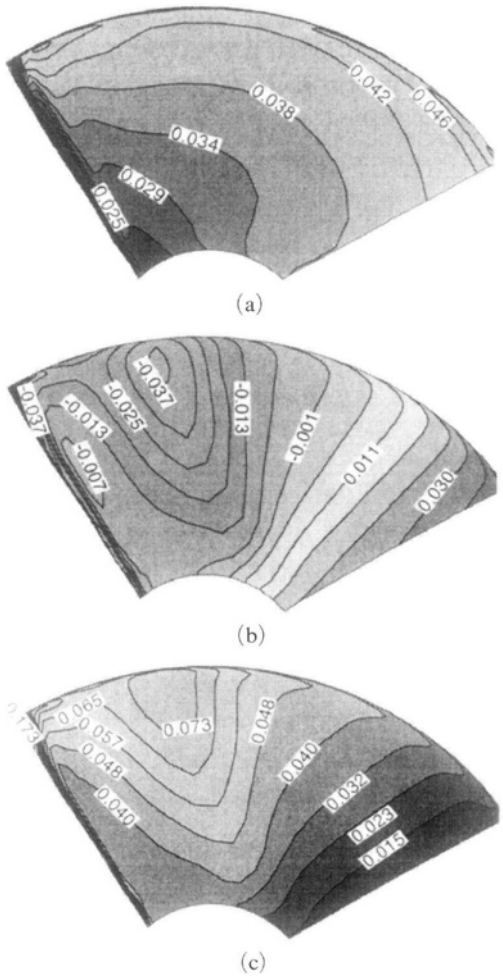

Fig. 19 Static pressure distributions on (a) Pressure and (b) Suction surfaces and (c) Blade loading of the radial model ; $\phi=0.078$

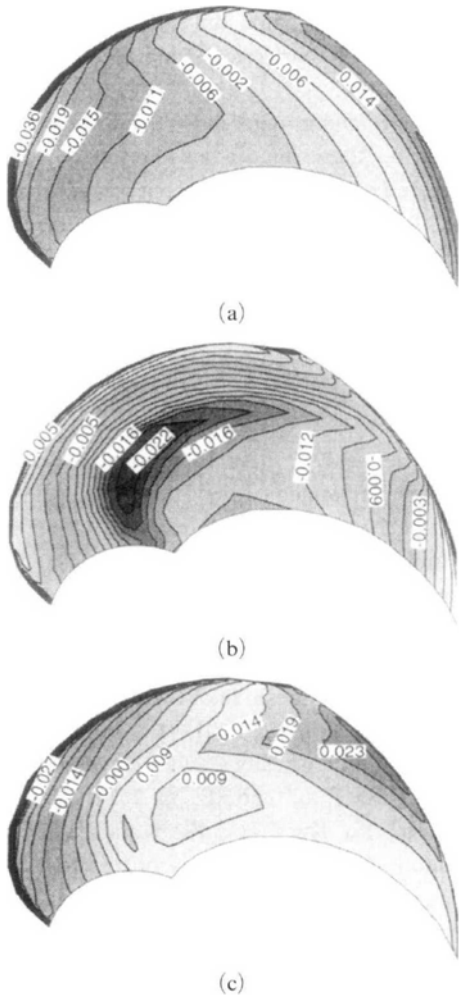

Fig. 20 Static pressure distributions on (a) Pressure and (b) Suction surfaces and (c) Blade loading of the backswept model ; $\phi=0.078$

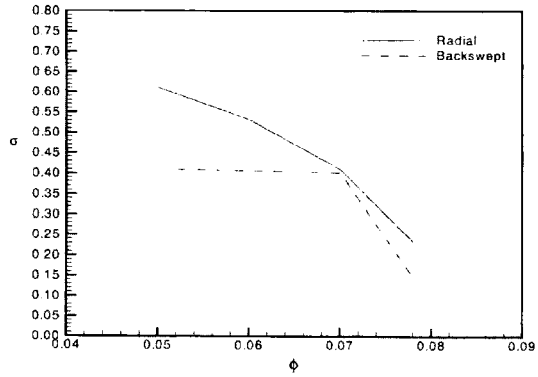

Fig. 21 Variation of cavitation numbers with flow rates

For the backswept model, pressure on the pressure surface gradually increases from values of -0.036 near the leading edge to the downstream as shown in Fig. 20(a), while the pressure on the suction side gradually increases after showing its minimum value of -0.022 near the mid span as shown in Fig. 20(b). Iso-pressure lines are parallel to the leading edge for this case. The blade loading has its maximum value 0.173 at the tip of leading edge for the radial type. But for the backswept inducer, the pressure difference is -0.027 near leading edge and becomes positive value at the downstream in Fig. 20(c), so that it has much lower blade loading than that of the radial type.

From the minimum value of pressure on the suction surface, usually at the tip leading edge, the cavitation inception number can be obtained and shown in Fig. 21. The values decrease with the flow rate. As the flow rate decreases, the incidence angle increases and the cavitation number increases. Backswept leading edge reduces the values. It means that cavitation inception delays for the backswept vane.

4. Conclusion

Performance and through flows of two inducer models of a turbopump are evaluated using a Navier-Stokes code, CFX-Tascflow for various flow rates.

Calculated results show good coincidence with experimental data of static pressure performance and velocity profile over the leading edge for the radial inducer.

Upstream recirculation, tip leakage flow and vortex flow, occurred at the blade tip and near leading edge, are main sources of pressure loss. Pressure loss from the upstream to the leading edge is almost equal amount to that of pressure loss through the blade passage. The total viscous loss is considerably large due to the strong secondary flow.

There appears more stronger leading edge recirculation for the backswept inducer, and this increases the pressure loss. However, blade loading near the leading edge and cavitation inception

number are considerably reduced.

Acknowledgment

The authors wish to thank Professor Tsujimoto and Yoshida of Osaka University for supplying experimental data and kind technical discussion. Present study was supported by Hyundai Mobis Co. through the MOST research program.

References

AEA Technology, 1999, CFX-TASCflow user's documentation, version 2.9.

George Bache, 1994, "Navier-Stokes Computations for The Complex 3D Flow Fields of Inducers and Centrifugal Impellers," Fifth Int. Symp. on Transport Phenomena and Dynamics in Rotating Machinery, May.

Howard, J. H. G., Tropea, C., Almahroos, H. M. H. and Roeber, T. W., 1987, "LDV Measurements of the Axial Velocity Field Within and Ahead of an Axial Pump Inducer at Off-Design Flow Rate," Proceedings of the ASME/JSME Thermal Engineering Conference, Vol. 2, pp. 63~69.

Jackson, E. D. and Cook, R. M., 1983, "Test of SSME Low Pressure Pump in Liquids at Zero Throughflow," ASME, Performance Characteristics of Hydraulic Turbines and Pumps, pp. 179~185.

Moore, J., Doan, Andrew, W. and Moore, Joan G., 1995a, "Performance Evaluation of Rocket Pump Inducers Using a Navier-Stokes Flow Code. Part 1 : 3-D Flow and Inlet Recirculation," FED-Vol. 227, Numerical Simulations in Turbomachinery.

Moore, J., Doan, Andrew, W. and Moore, Joan G., 1995b, "Performance Evaluation of Rocket Pump Inducers Using a Navier-Stokes Flow Code. Part 2 : Work Contributions and Pump Characteristics," FED-Vol. 227, Numerical Simulations in Turbomachinery.

Moore, J., Le Fur, T. and Moore, J. G., 1990, "Computational Study of 3-D Turbulent Air Flow in a Helical Rocket Pump Inducer," AIAA Paper 90-2123.

Tanaka, T., 1980, "An Experimental Study of Backflow Phenomena in a High Specific Speed Propeller Pump," ASME Paper No, 80-FE-6.

Tsujimoto, Y. and Yoshida, Y., 1998, "Flow Field Measurement at Inlet of 4 Bladed Inducer Using LDV," Domestic Report of Osaka University.

Tsujimoto, Y., Yoshida, Y., Acosta, A. J., Azuma, S. and Laffite, S., 2001, "Effects of Leading Edge Swept on Unsteady Cavitation in Inducers," Trans. of JSME, 67(656) B, pp. 903~910.

Yokota, K., Kurahara, K., Kataoka, D. and Tsujimoto, Y., 1999, "A Study of Swirling Backflow and Vortex Structure at the Inlet of an Inducer," JSME International Journal, Series B, Vol. 42. No. 3.

Yoshida, Y., Tsujimoto, Y., Kataoka, D. et al., 2000, "Effects of Alternate Leading Edge Cutback on Unsteady Cavitation in 4-Bladed Inducers," FED SM2000-11034.